Sains Malaysiana 54(8)(2025): 1927-1944
*http://doi.org/10.17576/jsm-2025-5408-05*

# A Series of Modified Mordenite for Green Fuel Production from Oleic Acid

(Suatu Siri Mordenit Terubah Suai untuk Pengeluaran Bahan Api Hijau daripada Asid Oleik)

KHOIRINA DWI NUGRAHANINGTYAS[1,*], SOFIA AULIA MUKHSIN[1], RIZKI LUKITAWATI[1], FITRIA RAHMAWATI[1], I F NURCAHYO[1], ENY KUSRINI[2,3,4] & YUNIAWAN HIDAYAT[1]

[1]*Department of Chemistry, Faculty of Mathematics and Natural Sciences, Sebelas Maret University, Jl. Ir. Sutami 36A, Surakarta, Indonesia*
[2]*Department of Chemical Engineering, Faculty of Engineering, Universitas Indonesia, Kampus Baru UI Depok, 16424, Indonesia*
[3]*Research Group of Green Product and Fine Chemical Engineering, Laboratory of Chemical Product Engineering, Department of Chemical Engineering, Universitas Indonesia, Kampus Baru UI, Depok, 16424, Indonesia*
[4]*Tropical Renewable Energy Research Center, Faculty of Engineering, Universitas Indonesia, Kampus Baru UI, Depok, 16424, Indonesia*

*Received: 25 December 2024/Accepted: 23 June 2025*

ABSTRACT

Green diesel and biogasoline are low-oxygen compounds in green fuel. Palm oil is a potential source of green fuel production through a hydrodeoxygenation reaction assisted by a specific catalyst. In this research, a series of transition metal (i.e., Fe, Co, Ni, Cu, and Zn) deposited in mordenite (MOR) catalysts were investigated for the hydrodeoxygenation reaction. Oleic acid was used to represent palm oil. All catalysts can convert oleic acid into green fuel products, particularly straight-chain alkane hydrocarbons with low free oxygen content. The Co/MOR catalyst converted 98.82% of oleic acid with a 76% selectivity for green fuel. The performance of the catalyst in one period follows the Sabatier Principle for the catalyst rather than the periodic system of elements.

Keywords: Biogasoline; green diesel; hydrodeoxygenation; mordenite; transition metal

ABSTRAK

Disel hijau dan biogasolin adalah sebatian oksigen rendah dalam bahan api hijau. Minyak sawit merupakan sumber berpotensi pengeluaran bahan api hijau melalui tindak balas hidrodeoksigenasi yang dibantu oleh mangkin tertentu. Dalam penyelidikan ini, satu siri logam peralihan (iaitu, Fe, Co, Ni, Cu dan Zn) yang dimendapkan dalam mangkin mordenit (MOR) telah dikaji untuk tindak balas hidrodeoksigenasi. Asid oleik digunakan untuk mewakili minyak sawit. Semua pemangkin boleh menukar asid oleik kepada produk bahan api hijau, terutamanya hidrokarbon alkana rantai lurus dengan kandungan oksigen bebas yang rendah. Pemangkin Co/MOR menukarkan 98.82% asid oleik dengan selektiviti 76% untuk bahan api hijau. Prestasi pemangkin dalam satu tempoh mengikut Prinsip Sabatier untuk pemangkin dan bukannya sistem unsur berkala.

Kata kunci: Biogasolin; disel hijau; hidrodeoksigenasi; logam peralihan; mordenit

## INTRODUCTION

Green diesel and biogasoline have long been recognized as an ecologically beneficial alternative to fuel, a non-oxygen hydrocarbon molecule derived from vegetable oil (Asikin-Mijan et al. 2023; Kamaruzaman, Taufiq-Yap & Derawi 2020). Green diesel comprises straight and branching saturated hydrocarbon chains with 13 to 18 carbon atoms per molecule (C13-C18), while biogasoline comprises hydrocarbon chains with 4 to 12 carbon atoms per molecule(C4-C12) (Pazmiño-Viteri et al. 2024). Because its composition is similar to fuel, green diesel, and biogasoline may be used as a green fuel in engines in its pure form or as a mixture with the necessary mixing ratio without engine modifications (Douvartzides et al. 2019). As an alternative fuel, green fuel may save 66-84% of fossil fuels while reducing greenhouse gas emissions by 42-85% (Ajeeb et al. 2025; Orozco et al. 2017).

Oleic acid may be used as a model chemical since it is the principal component of vegetable oils, such as palm oil, rapeseed oil, and castor oil, at concentrations of 45%, 63%, and 38.9%, respectively. Oleic acid's chemical formula is $C_{18}H_{34}O_2$, representing double bonds and carboxylic acid groups in vegetable oils (Carli, Susanto & Habibie 2018; Haryani et al. 2020). Furthermore, oleic acid contains long-

chain fatty acids suited for creating highly selective green fuel fractions via the hydrotreatment process (Nugraha et al. 2024; Nur Azreena et al. 2021).

Green fuel is made from triglycerides using a hydrotreatment reaction, resulting in a mixture of alkanes with carbon numbers in the range of diesel and gasoline (Asikin-Mijan et al. 2023; Morgan et al. 2024; Nugraha et al. 2024; Puspawiningtiyas et al. 2022; Siraj & Ceylan 2025; Taromi & Kaliaguine 2018). The hydrotreatment method is divided into three stages: hydrodeoxygenation (HDO), decarbonylation (DCO), and decarboxylation ($DCO_2$) (Nur Azreena et al. 2024). HDO is an exothermic process that removes oxygen from triglyceride molecules like $H_2O$, whereas DCO and $DCO_2$ are moderate endothermic reactions that remove oxygenate molecules like CO, $H_2O$, and $CO_2$, respectively (Wang et al. 2018).

The hydrotreatment process for removing the carbonyl group in aromatic compounds needs a catalyst so that the reaction can run quickly and effectively and obtain optimal results (Jing et al. 2018). The metals used as catalysts in this study are first-period transition metals (TMs) because they can provide an active site in their d orbitals (Janampelli & Darbha 2019). Its performance is comparable to that of precious metals, and the waste generated is more environmentally friendly (Carli, Susanto & Habibie 2018).

The TMs elements have different catalytic properties due to the varying electronic properties of the d orbitals (Kordulis et al. 2016). Fe metal has several unoccupied d orbitals that can bind $H_2$, a high electronic affinity, and a wide range of oxidation numbers. So, Fe metal can inhibit the production of carbonyl compounds (Arun, Sharma & Dalai 2015; Luciano et al. 2022; Neonufa et al. 2019). Cobalt metal possesses an active site with acidic characteristics, which can improve catalytic performance. Cobalt has selectivity for linear hydrocarbons to remove oxygen, reduce coke formation, and slow deactivation (Ayodele 2017). Nickel metal has an active site for fast-absorbing $H_2$ with low hydrogen dissociation energy. In addition, nickel also has decarboxylation and decarbonylation activities (Aliana-Nasharuddin et al. 2019; Arun, Sharma & Dalai 2015; Hafriz et al. 2020; Hongloi et al. 2019; Jeon et al. 2019a). Meanwhile, Cu metal has a d orbital full of electrons, and a 4s orbital is half full ($3d^{10}4s^1$), so Cu metal has low surface free energy (Miao et al. 2020). Zn metal has attractive properties for the production of aromatic compounds (Pourzolfaghar et al. 2020; Zhao et al. 2015). Meanwhile, nickel metal elements ($Ni^0$) perform better for green diesel production than metal oxides (Hongloi, Prapainainar & Prapainainar 2022).

Several studies on green fuel production with zeolite-based transition metal catalysts have been conducted, including HY-based for TMs, H-ZSM-5-based for Ni, and NiMo with beta zeolite and USY as a support (Choo et al. 2020; Hongloi et al. 2019). Because these supporting components have a high strength acidity level, their role in catalyzing light hydrocarbons and producing biogasoline is more active (Li et al. 2020). High strength acid levels can also produce coke deposition to degrade the catalyst's active site (Hafriz et al. 2020; Safa Gamal et al. 2020).

Mordenite (MOR) has not yet been investigated entirely as a heterogeneous support catalyst in green fuel production. MOR is the most abundant component (up to 70%) of Indonesian natural zeolites, which have mildly acidic properties compared to other zeolites such as HY, H-ZSM-5, beta zeolite, and USY. Due to this mild acidity, hydrocracking (HC) processes can be avoided, resulting in properties that are superior to those of other zeolites. Furthermore, MOR has a large pore size (±7 Å), a structure with cavities and channels, and high thermal stability, making it suitable for catalyst support (Oyedotun 2018; Panchuk et al. 2018). Based on these ideas, it is required to investigate the activity and selectivity of first-period transition metal catalysts (Fe, Co, Ni, Cu, and Zn) impregnated in MOR to produce green fuel.

## MATERIALS AND METHODS

### MATERIALS

Double distilled water was purchased from PT. Ikapharmindo Putra Ma), Whatman 42 filter paper, $N_2$, and $H_2$ gas with purity >98% (PT. Samator Indonesia), Oleic acid, $NH_3$ 25%, and metal nitrate salts of Fe, Co, Ni, Cu, and Zn as catalyst precursors supplied by E Merck (Germany). Meanwhile, without purification, HS-690 type mordenite was purchased from FUJIFILM Wako Chemical Corporation from E Merck (Germany).

### CATALYST PREPARATION AND CHARACTERIZATION

TMs-modified MOR (Fe, Co, Ni, Cu, and Zn) was prepared by impregnating methods. The procedure in this study refers to our previous study, where the metal content has been optimized (Mazlan, Nugrahaningtyas & Rahmawati 2022; Nugrahaningtyas, Putri & Saraswati 2020; Nugrahaningtyas et al. 2022b). The first step was to mix 0.02 mol of nonahydrate iron (III) nitrate precursor salt per weight of zeolite. MOR, then was soaked in 25%w ammonia, followed by distilled water twice until the total volume reached 200 mL. Furthermore, the mixture was refluxed in two stages: refluxing at 30 °C for 16 h and then followed by reflux at 80 °C for 4 h. For other metal-modified MOR, each precursor metal salt was also introduced to the same protocol to obtain Co/MOR, Ni/MOR, Cu/MOR, and Zn/MOR. After impregnation, the sample was filtered and dried for one week at room temperature and then evaporated using a rotary evaporator at 0.21 atm and 68.9 C until powder. The following process is catalyst activation, which includes calcination at 550 °C for 3 h under $N_2$ gas and reduction under gas at 400 °C for 2 h, with a 15 mL/min flow rate. The catalyst obtained is called Fe/MOR. The Fe/Mor manufacturing process was repeated with different precursor salts to obtain Co/MOR, Ni/MOR, Cu/Mor, and Zn/Mor catalysts.

Each sample was characterized by its metal phase, metal content, textural, and acidity. The results of diffraction patterns, metal phases, and crystal structure analysis using XRD have been reported in our previous publications (Nugrahaningtyas et al. 2022b). The analysis with XRF (Bruker S2 Ranger) to prove the presence of metal bound to MOR. Metal content was obtained from analysis using XRF by utilizing X-rays emitted by the TMs/MOR catalyst sample, which was then captured by the detector to analyze the metal and elemental content in the sample. The texture of the catalyst viz surface area, total pore volume, and the average pore radius of the TMs/MOR catalyst was analyzed using an SAA (Quanta chrome Nova Win) based on isotherm adsorption $N_2$ gas with pretreatment, i.e., degassing at 300 °C for 3 h. The acidity of the TMs/MOR catalyst was analyzed by TPD using $NH_3$ as a probe molecule and thermal conductivity detector (TCD) as a detector.

### HYDRODEOXYGENATION OF OLEIC ACID

The first step of HDO of oleic acid was to make tube-like pellets of Fe/MOR with a diameter of 2 cm and a weight of 5 mg using catalyst pelletizing (Edu lab). Then, the Fe/MOR pellets were put into a semi-flow reactor (Edu lab) and heated at 350 °C under $H_2$ gas. The next step involved streaming oleic acid vapor and hydrogen gas at a flow rate of 15 mL/min. Then, the products were collected and identified using GCMS (GC-MS Shimadzu QP 2010 SE). The repeated activity test steps for Co/MOR, Ni/MOR, Cu/MOR, and Zn/MOR catalysts. The Yield, conversion of oleic acid (activity of catalyst), and selectivity of catalyst were calculated according to our previous paper (Choo et al. 2020; Hafriz et al. 2020; Nugrahaningtyas et al. 2022a, 2018). The activity and selectivity values indicate the ability of a catalyst, where the activity value represents the percentage of reactants converted into products (percentage conversion). Meanwhile, the selectivity value is the percentage of the desired product compared to the total number of products.

$$\textit{Yield (\%) = (percentage area of product)} \times \frac{\text{total product volume}}{\text{initial rectant volume}} \quad (1)$$

$$\textit{Conversion (\%)} = \frac{\text{(Mass of feed) initial} - \text{(Mass of feed) final}}{\text{(Mass of feed) initial}} \times 100\% \quad (2)$$

$$\textit{Biogasoline Selectivity (\%)} = \frac{\text{Total percentage area of Hydrocarbon C8} - \text{C12}}{\text{Total percentage area of hydrocarbon product}} \times 100\% \quad (3)$$

$$\textit{Greendiesel Selectivity (\%)} = \frac{\text{Total percentage area of Hydrocarbon C13} - \text{C18}}{\text{Total percentage area of hydrocarbon product}} \times 100\% \quad (4)$$

### ELEMENTAL OXYGEN ANALYSIS

The composition of chemical compounds in the reaction product was analyzed by GCMS. Meanwhile, the oxygenated removal efficiency (%) was calculated using Equations (5) adopted from previous research with modifications, in accordance with the GCMS data (Hafriz et al. 2020).

$$\textit{Oxygenated removal efficiency (\%)} = \frac{Af - Ap}{Af} \times 100\% \quad (5)$$

where

*Af* : $\sum$ *percentage area of oxygenated compound of feed* ; and

*Ap* : $\sum$ *percentage area of oxygenated compound of product*

## RESULTS AND DISCUSSION

### PHYSICAL AND CHEMICAL CHARACTERISTICS OF CATALYST

The crystallinity, phase type, and crystal structure of mordenite were determined based on XRD data (Figure 1). Further analysis was carried out by refining the XRD diffraction pattern using the Le Bail method with RIETICA software (supplementary file 1). The first refinement was conducted to find the suitability between the mordenite carrier and the existing mordenite standard based on the residual factor values (Rp and Rwp). The standards with the highest suitability were the ICSD #4393 and ICSD #4394 mordenite standards. Based on ICSD #4393 data, mordenite has a *Cmcm* space group symmetry, an orthorhombic crystal system, lattice parameters a = 18.007 Å; b = 20.269 Å; c = 7.465 Å, angle between axes α=β=γ=90° and cell volume: 2724.6 $Å^3$. Meanwhile, based on the ICSD #4394 standard, mordenite has a *Cmcm* space group symmetry, an orthorhombic crystal system, lattice parameters a = 18.2230 Å; b = 20.465 Å; c = 7.531 Å, an angle between axes α=β=γ=90° and a cell volume of 2808.56$Å^3$.

The next stage involves analyzing crystallinity, phase type, crystal structure, and verifying the success of mordenite modification using XRD. There is no significant difference in the peak position and diffractogram pattern, indicating that the crystallinity of mordenite remains intact after metal addition (Figure 2). The decrease in the intensity of the characteristic peaks of mordenite of each catalyst indicates that the loaded metals cover the surface of mordenite. Following previous studies, this

decrease in characteristic peak intensity is also associated with compositional changes in mordenite due to cation exchange (Sakizci & Kılınç 2015). Further analysis was carried out by refining the XRD diffraction pattern of the TMs/mordenite sample. The results of the Le Bail plot of all catalysts with all standards are shown in Supplementary File 2.

Based on the refinement results (Table 1), it can be seen that adjusting the sample data with standard data (ICSD #4393 and #4394) can cause changes in cell parameters. These changes occur in the lattice parameters (a, b, c) and cell volume. The residual factor value in all samples is below 10%, indicating that the suitability of sample data with mordenite standard data (ICSD #4393 and #4394) is still acceptable.

Refinement analysis can also determine the metal phases of the TMs/MOR catalyst with standard data for each metal and its oxide phase. Standard metal data that match the TMs/MOR sample are presented in Table 2. Transition metals are supported on mordenite in both oxide and elemental phases (Table 3). It can be seen that the molar percentage of TMs/MOR varies from 0.04% to 1.26%, depending on the type of metals. As previously found, not all TM can attach to mordenite, whereas Fe metal is mostly attached to mordenite (Nugrahaningtyas, Putri & Saraswati 2020; Nugrahaningtyas et al. 2022b).

Iron is most abundantly bound to MOR because its Ksp value is the lowest among the transition metals. In addition, since the support surface is negatively charged during the preparation of the catalyst in basic conditions, the surface is more likely to adsorb positively charged metal ions. As a result, Fe metal diffuses rapidly to the surface. Since Fe metal has a higher positive charge than other first-row transition metals, it is easier to bind to the support. Table 4 shows that the surface area has been reduced by 13 to 37% due to metal impregnation, which can cover the support surface. The decrease in the surface area of the catalyst will harm its catalytic activity (Nugrahaningtyas et al. 2021). On the other hand, the presence of metal attempts to produce a new active site in the form of a Lewis acid site, which could also compensate for the lower activity caused by a decrease in the surface area of the supporting material (Zheng et al. 2020).

Based on SAA data, the impregnation of Co substantially increased by 18% of the pore width and 2% of the pore volume of the MOR (Table 4). The wide surface area shows cobalt is more uniformly spread than other catalysts. Cobalt is exposed and functions as an active site on the catalyst. The more active and accessible the sites, the more possible interactions between reactants and catalysts exist. Consequently, the reactant is easier to activate, resulting in a more effective reaction and more products. Meanwhile, the adsorption-desorption isotherms of all catalysts lead to a type IV isotherm, with a different hysteresis pattern (Figure 3). Type IV adsorption isotherms arise from porous solid materials with a mesoporous size between 2-50 nm and 0.002-0.05 m (Bardestani, Patience & Kaliaguine 2019). Hysterical widening at a high P/Po between 0.4 and 0.9 simultaneously indicated the presence of a mesoporous. The hysterical widening indicates that more $N_2$ gas left the pores during desorption. As a result, the size of the mesoporous becomes large. In this study, the Co/MOR catalyst showed a relatively sizeable hysterical dilation compared to other catalysts, so it indicated that the mesoporous size of the Co/MOR catalyst was relatively large.

Previous studies have shown that with mesoporous size support, the catalyst can produce high activity in fatty acid HDO reactions because they offer suitable pore diameters required for the diffusion of fatty acid molecule (Arun et al. 2021; Crawford et al. 2020). Oleic acid has a molecular diameter of 2–30 nm, while the catalysts in this study have a pore diameter of 2-50 nm. It is clear that Oleic acid's size fits with the catalyst's pore.

The number and the strength of the acid sites are measured using the $NH_3$-TPD instrument. The desorption area shows the acid content, whereas the large desorption area represents more acidity properties. As seen in Figure 3, the MOR has higher acidity, which means that the acidity decreases after added metals. The decrease in acid number by 16%-42% is due to the dispersion of metal species (Fe, Co, Ni, Cu, and Zn) on the MOR surface, which blocks and limits the accessibility of $NH_3$ to the catalyst pores. As stated by Nur Azreena et al. (2021) and Zheng et al. (2020), these dispersions could cover the Bronsted acid site or drive the cation exchange with the Bronsted acid. As a consequence, the catalyst loses its acidity. Based on the acidity character, the data shows that from left to right, the TM acidity value tends to decrease, namely to the minimum value, from Fe/MOR (574 μmol/g) and Co/MOR (390 μmol/g) to Ni/MOR (393 μmol/g), then increases for the Cu/MOR catalyst (570 μmol/g) and slightly decreases for the Zn/MOR catalyst (466 μmol/g). Meanwhile, the Cu/MOR catalyst has the highest acid number and the strongest acid site compared to other catalysts. This phenomenon may be due to the strong interaction between copper and MOR, so that Cu metal is better dispersed compared to other catalysts. The order of the acidity number of the catalyst is as follows: Cu/MOR> Zn/MOR> Co/MOR> Ni/MOR> Fe/MOR.

The acid strength of the catalyst is directly proportional to the catalyst's ability to release ammonia. The stronger the acidity properties, demanding higher temperature (>500 °C) to desorb ammonia, the otherwise observed response at low temperatures (<280 °C) indicates that ammonia is adsorbed at a weak acid site (Nur Azreena et al. 2021). Transition metals contain d orbitals that are not entirely occupied by electrons, allowing them to bind ammonia. The binding force for ammonia increases as the d orbital becomes more vacant, and vice versa. The ammonia desorption peak at a high temperature represents the Bronsted acid site. The peak of ammonia desorption at low temperatures describes the interaction of ammonia with Lewis's acid sites (Chen et al. 2019).

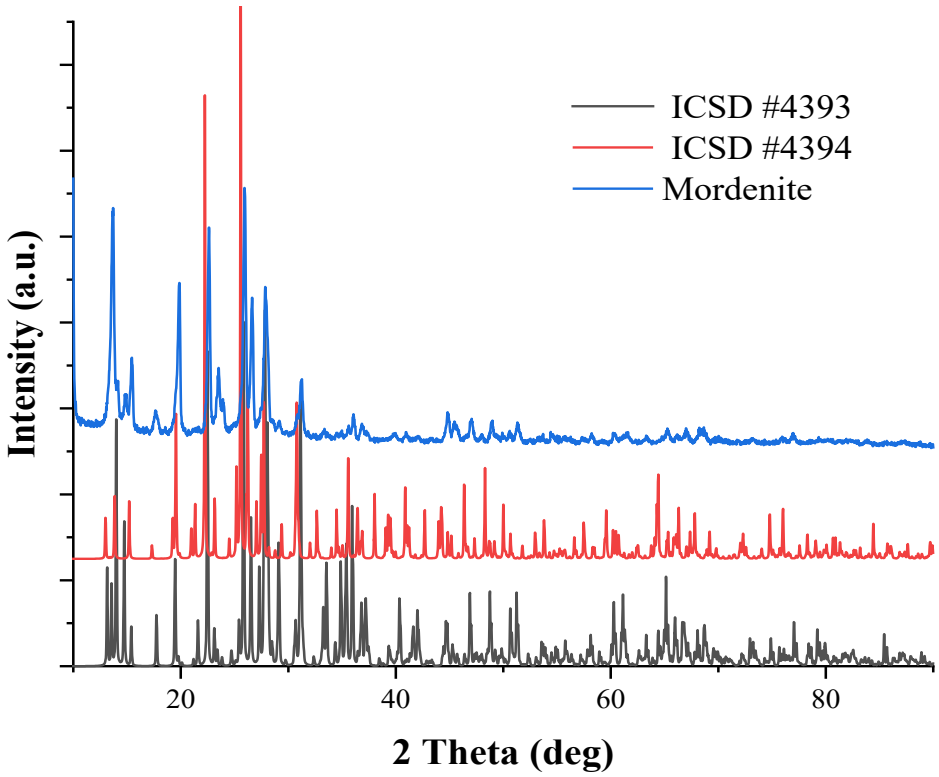


FIGURE 1. Diffraction patterns of mordenite and mordenite standards (ICSD #4393 and ICSD #4393)

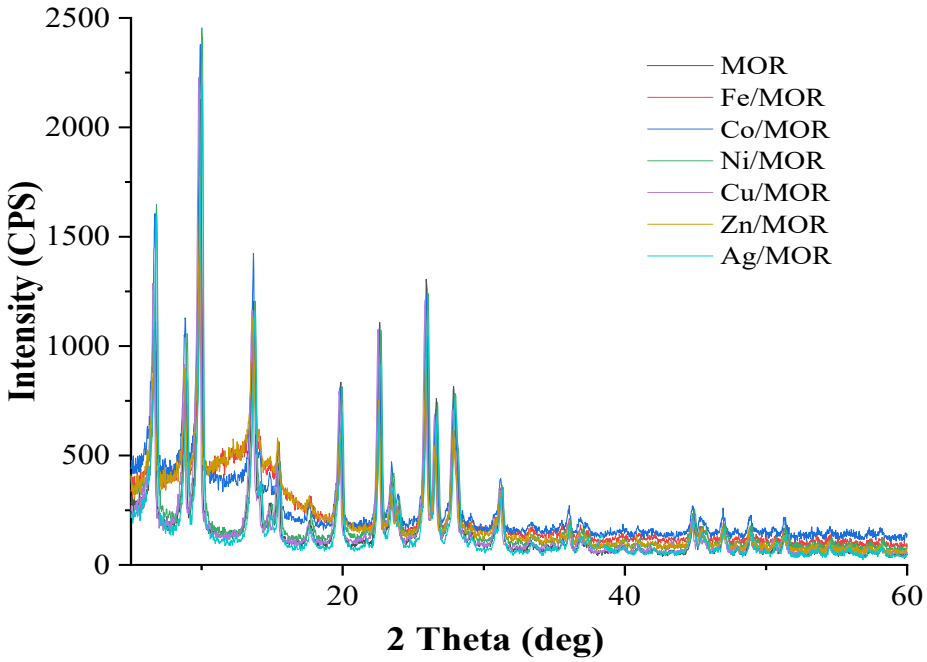


FIGURE 2. The diffraction patterns comparison of mordenite and TMs/ mordenite

TABLE 1. Refinement results using mordenite standards (ICSD #4393 and #4394)

| Cell Parameter | MOR | Fe/MOR | Co/Mor | Ni/ MOR | Cu/ MOR | Zn/ MOR |
|---|---|---|---|---|---|---|
| Crystal Structure | Ortho-rhombic | Ortho-rhombic | Ortho-rhombic | Ortho-rhombic | Ortho-rhombic | Ortho-rhombic |
| Space Group | *C m c m* | *C m c m* | *C m c m* | *C m c m* | *C m c m* | *C m c m* |
| a (Å) | 17.649 | 17.910 | 17.381 | 16.410 | 17.763 | 17.815 |
| b (Å) | 19.746 | 20.165 | 19.487 | 18.56 | 19.875 | 19.888 |
| c (Å) | 7.257 | 7.481 | 7.181 | 6.871 | 7.299 | 7.345 |
| Angles (∘) | α=β=γ=90 | α=β=γ=90 | α=β=γ=90 | α=β=γ=90 | α=β=γ=90 | α=β=γ=90 |
| Cell Volume(Å$^3$) | 2529 | 2702 | 2432 | 2115 | 2577 | 2602 |
| Z | 48 | 48 | 48 | 48 | 48 | 48 |
| Rp (%) | 5.89 | 6.10 | 4.71 | 7.85 | 5.61 | 6.48 |
| Rwp (%) | 5.13 | 5.64 | 5.12 | 6.98 | 5.27 | 6.10 |

TABLE 2. The standard data of metal phase corresponding to TMs/MOR sample

| TMs/MOR | Fe/MOR | Co/Mor | Ni/ MOR | Cu/ MOR | Zn/ MOR |
|---|---|---|---|---|---|
| Metal Element | Fe (ICSD#41506) | Co (ICSD#41507) | Ni (ICSD#41508) | Cu (ICSD#53247) | - |
| Metal Oxide | $Fe_2O_3$ (ICSD#51122) | CoO (ICSD#43458) | NiO (ICSD #92127) | CuO (ICSD#61323) | ZnO (ICSD#57156) |

TABLE 3. Molar weight percentage of mordenite and catalyst TMs/MOR

| Phase | Molar weight percentage (%) | | | | | |
|---|---|---|---|---|---|---|
| | MOR | Fe/MOR | Co/Mor | Ni/ MOR | Cu/ MOR | Zn/ MOR |
| MOR (ICSD #4393) | 48.59 | 48.18 | 48.44 | 49.36 | 48.48 | 49.24 |
| MOR (ICSD #4394) | 51.41 | 50.49 | 51.46 | 50.53 | 51.34 | 50.64 |
| Metal Element | - | 0.06 | 0.06 | 0.06 | 0.07 | - |
| Metal Oxide | - | 1.26 | 0.04 | 0.06 | 0.11 | 0.12 |

TABLE 4. The characteristics of TMs/MOR catalyst (TMs = Fe, Co, Ni, Cu, and Zn)

| Catalyst | Metal content (mmol/g) | Specific surface area (m$^2$/g) | Pore diameter (Å) | Pore volume (cc/g) | Acidity (μmol/g) |
|---|---|---|---|---|---|
| MOR | 0 | 526 | 16.1 | 0.425 | 680 |
| Fe/MOR | 11.7 | 369 | 16.7 | 0.307 | 574 |
| Co/MOR | 7.2 | 456 | 19.0 | 0.434 | 390 |
| Ni/MOR | 9.3 | 412 | 15.8 | 0.326 | 393 |
| Cu/MOR | 7.1 | 404 | 14.7 | 0.297 | 570 |
| Zn/MOR | 1.4 | 334 | 24.2 | 1.365 | 466 |

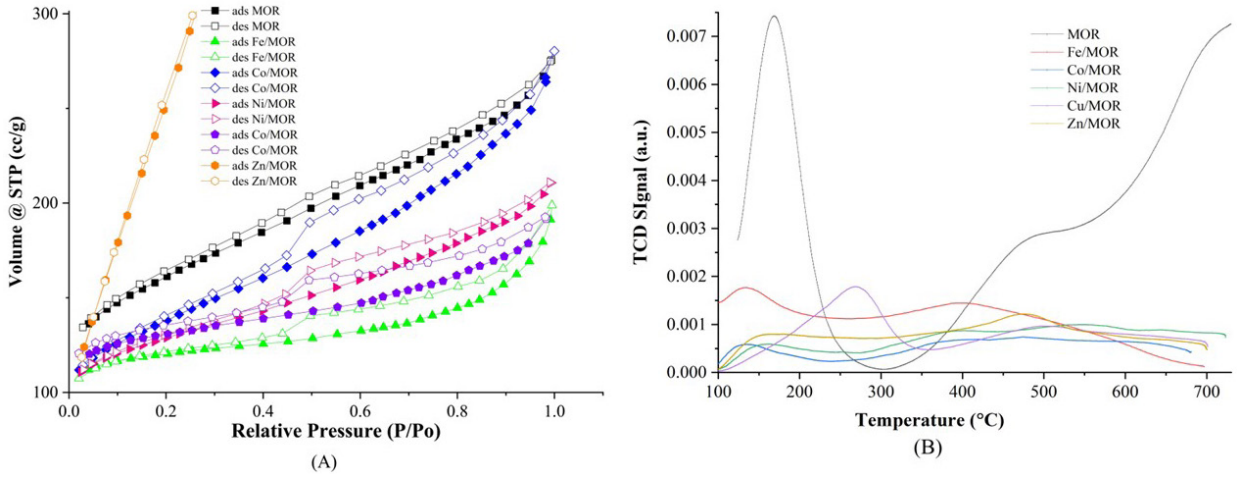


FIGURE 3. (A) Adsorption-Desorption Isotherm of $N_2$ Gas on TMS/ MOR Catalyst and (B) TPD pattern of TMs/ MOR catalyst (TMs = Fe, Co, Ni, Cu, and Zn)

The Fe/MOR catalyst has a more prominent metal content than other catalysts, resulting in the most acidic properties. Unfortunately, the high metal content was thought to cover or displace the Bronsted acid site of the support, so the catalyst was dominated by the Lewis acid site of the metal, as indicated by the ammonia desorption peak at low temperature (<280 °C) (Chen et al. 2019; Zheng et al. 2020). The study is the same as previous studies' results, which stated that the catalyst with the highest number of metals increased acidity in the form of Lewis acid sites from metals with weaker acid strengths. In line with this phenomenon, the low strength of Fe/MOR acid is predicted to decrease the catalytic activity (Nur Azreena et al. 2021).

Meanwhile, the Co/MOR catalyst showed the smallest desorption peak area at moderate temperatures, namely 350-500 °C. Based on the interpretation of the $NH_3$-TPD data, the Co/MOR catalyst has the lowest total acidity with moderate acid strength. Same as Fe/MOR, the lowest total acidity with a moderate acid strength of Co/MOR catalyst can affect HDO activity (Arun et al. 2021). The Ni/ MOR catalyst showed three desorption peaks at different temperatures, i.e., at 150, 400, and 550 °C. One of the desorption peaks appeared at a temperature of 150 °C, which is lower than the other two desorption peaks in the medium-temperature range, around 400 °C and 550 °C. The interpretation of the $NH_3$-TPD data indicates that the acidity of the Ni/MOR catalyst is moderate. The moderate acid strength of Ni/MOR can reduce the occurrence of HC reactions and can optimize the reaction for breaking the bonds of oxygenate compounds.

The Cu/MOR catalyst showed two desorption peaks in the low and moderate-temperature regions, i.e., at 275 and 500 °C, which indicated that the Cu/MOR catalyst had low and moderate acidity strength. It is predicted that the Cu/MOR catalyst increased the cleavage of the oxygenated compound in the hydrodeoxygenation reaction. The Zn/ MOR catalyst also showed two desorption peaks in the low-temperature and moderate-temperature regions. The interpretation of the $NH_3$-TPD data shows that the Zn/ MOR catalyst has moderate acidity but is close to high acidity compared to other TMs/MOR catalysts. The area of the desorption peak that appears in the medium temperature area is larger than the area of the desorption peak that appears at low temperature. The moderate acidity strength with a large amount of the Zn/MOR catalytic acid site indicates high catalytic activity and oxygen removal efficiency. The high amount and strength of acid sites on Cu/MOR and Zn/MOR catalysts is the active centre for DO reactions of oxygenate compounds. The order of the acidity strength of the catalyst is as follows Ni/MOR > Cu/MOR > Zn/MOR > Co/MOR > Fe/MOR. The acid site mediates product selectivity by controlling decarboxylation and decarboxylation during deoxygenation reactions. However, the catalyst's highest acidity leads to a predominant HC reaction (Shim et al. 2015).

## THE CATALYTIC ACTIVITY OF TMs/MOR CATALYST (TMs = Fe, Co, Ni, Cu, AND Zn)

According to our previous research findings (Nugrahaningtyas et al. 2022c), MOR converts oleic acid more than 95% (Figure 4). The effectiveness of MOR is relevant to Rogers and Zheng's statement (Rogers & Zheng 2016). They concluded that MOR could act as support that provides a large surface area and plays a role in catalytic activity. MOR has a cavity and channel structure that supports its properties as a catalyst, and its large pores

can absorb oxygenated compounds. Compared to MOR, transition metals did not consistently improve conversion. However, Co/MOR and Zn/MOR gave better results than other catalysts.

The Co/MOR catalyst exhibits the maximum activity, as it can convert oleic acid to 98.82%. Even higher than the Co/ZSM-5 catalyst (80%) by other researchers (Ayodele 2017). High metal content and a large surface area play a significant role in converting oleic acid, which correlates to a more excellent dispersion of reactants to the active site (Shim et al. 2015). As the acid site strength improves from weak to moderate and the metal disperses better, the catalyst's activity will increase (Kochaputi et al. 2019). The weak acid sites prevent the catalyst from activating reactants and converting them into products, resulting in poor catalytic activity (Istadi et al. 2022). The addition of metal succeeded in increasing the yield of the liquid product in the thermal reaction, but the value was still lower than the MOR's yield, except for Ni/MOR. The smaller pore diameter and the acid strength of the TMs/MOR catalyst compared to MOR were unsuitable for interacting with oleic acid molecules, causing the liquid yield to decrease. The reason is that the pore diameter of Ni/MOR is similar to that of MOR, and Ni/MOR has moderate acidity strength.

The oxygen removal efficiency of TMs/MOR catalysts was checked using elemental analysis. The catalyst increased the efficiency of removing oxygen compounds compared to the thermal reaction (Table 5). The large oxygen-free product shows the high efficiency of the hydrodeoxygenation reaction (Zhang et al. 2019). The catalyst with the highest oxygen removal efficiency was the Zn/MOR catalyst, probably because the moderate acid strength of Zn was the greatest. This research agrees with the previous study, which states that moderate to high acidity will increase the bond-breaking reaction of the oxygenated compound (Arun, Sharma & Dalai 2015).

## LIQUID PRODUCT DISTRIBUTION IN DETAILS

The liquid yield from the conversion reaction of oleic acid can be grouped into carboxylic acids, alcohols, and hydrocarbons. Table 6 shows that the carboxylic acids predominate as intermediates, with alcohols appearing in trace quantities. Carboxylic acids consist of molecules with 4 to 18 carbons (C4-C18), with decanoic acid predominating in a large yield compared to other carboxylic acids. Decanoic acid ($C_{10}H_{22}O_2$) was known to be produced from the cracking reaction of the carbon double bond in oleic acid (Na et al. 2010).

Most catalysts produced alcohols with yields of 1.6 to 2.30 wt.%, except for the Cu/MOR catalyst, which had a high alcohol yield of 8.97 wt.%. According to de Oliveira Camargo et al. (2020), alcohol results from a continuous reduction of carboxylic acids with aldehyde as an intermediary. The dominance of carboxylic acid products over alcohol confirms that the hydrocracking process occurs more than the aldehyde reduction process.

Hydrocarbons compatible with the diesel fraction are the main product of the oleic acid HDO reaction. In total, 48-68% of oleic acid is converted to hydrocarbon, classifying into alkanes and alkenes. The respective products consist of C4-C12 and C13-C18, commercially known as biogasoline and green diesel (Mirzayanti et al. 2018). The low amount in the Bronsted acid sites of all TMs/MOR is responsible for the more significant alkene than alkane products. It indicates that the C=C double bond cleavage reaction does not dominate. These findings agree with others that alkane produced from the hydrogenation of C=C double bonds is influenced by the acidity of the Bronsted acid site (Jeon et al. 2019b). Consequently, the MOR with the most extraordinary Bronsted acidity provided the most alkane products.

The Zn/MOR catalyst has a relatively higher number of acidic sites with medium strength than other TMs/MOR catalysts (Shim et al. 2015). Therefore, the Zn/MOR catalyst, in addition to providing high oxygen removal efficiency, also provides high HC reaction activity. The large biogasoline yield indicates that the HC activity of the Zn/MOR catalyst is high (Figure 5(A)).

The results showed that the liquid product consisted of three compounds, namely carboxylic acids, alcohols, and hydrocarbons (Figure 5(B)). The product type indicates that the reaction of oleic acid HDO through three mechanisms, namely the $DCO_2$, DCO, and D-HDO pathways, follows previous studies (Choo et al. 2020; Prakhar et al. 2018). The high yield of the alkene product indicates that the $DCO_2$ reaction pathway is the main reaction pathway. These results are similar to the research of Choo et al. (2020), which stated that $DCO_2$ is oleic acid's main HDO reaction pathway.

## BIO GASOLINE AND GREEN DIESEL SELECTIVITY

Iron metal has high redox properties. Therefore, the Fe/MOR catalyst has a strong oxygen affinity and can bind oxygen from the C=O bond of oleic acid, thereby increasing the activity of the $DCO_2$ reaction (Neonufa et al. 2019; Zdainal Abidin et al. 2019). Other publications report that Co metal is suitable for hydrogenolysis reactions of C-O-C bonds. Thus, it can promote $DCO_2$ reactions (Arun, Sharma & Dalai 2015). Meanwhile, apart from having advantages in accelerating $DCO_2$ reactions (Aliana-Nasharuddin et al. 2019; Neonufa et al. 2019), Zn metals are also active for D-HDO reactions (Miao et al. 2020b), due to it is not found in DCO products.

This study is compatible with other research, where it found that the Co/MOR catalyst has the highest conversion value of 100%, while the selectivity of green diesel is the lowest (Ayodele 2017; Shim et al. 2015). The amount of biogasoline is smaller than green diesel, indicating that the HC reaction does not occur dominantly. The HC reaction is due to the high acidity of the catalyst. The strength of catalyst acidity improves the oxygen removal activity. However, the excessive acidity of the catalyst can cause

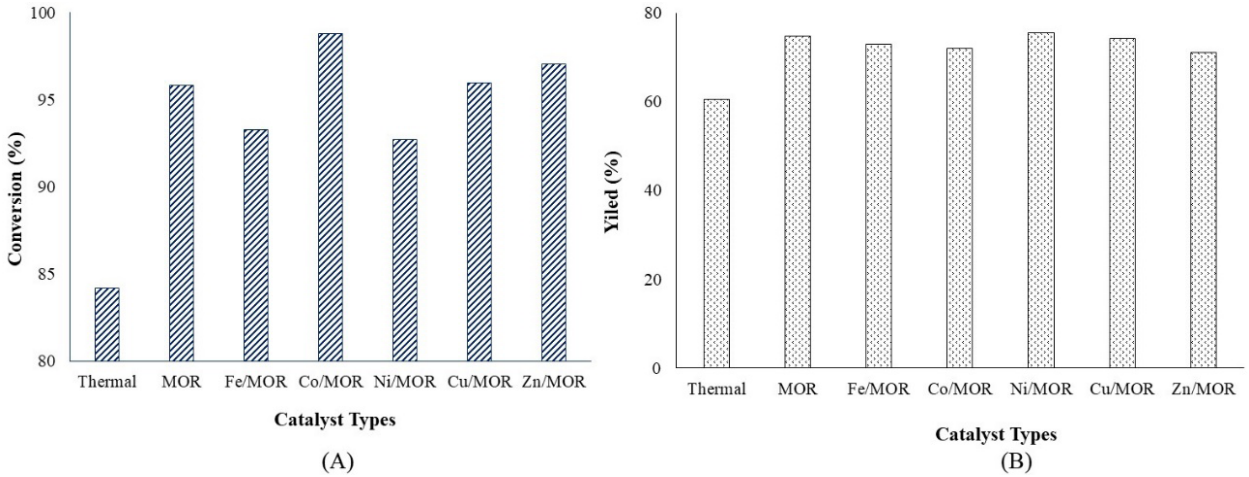


FIGURE 4. (A) Oleic acid conversion and (B) Yield of liquid product

TABLE 5. Oxygen contents of products and oxygen removal efficiency

| | Oxygen content (%) | Oxygen removal efficiency (%) |
|---|---|---|
| Oleic acid (feed) | 11.96 | - |
| Fe/MOR | 4.33 | 63.72 |
| Co/MOR | 4.49 | 62.41 |
| Ni/MOR | 4.29 | 64.05 |
| Cu/MOR | 4.01 | 66.45 |
| Zn/MOR | 3.38 | 71.68 |

TABLE 6. Liquid product composition of oleic acid HDO

| Yield (%) | Thermal | MOR | Fe/MOR | Co/MOR | Ni/MOR | Cu/MOR | Zn/MOR |
|---|---|---|---|---|---|---|---|
| Carboxylic acid | 16.59 | 12.04 | 17.48 | 0 | 16.46 | 14.30 | 11.16 |
| Alcohol | 2.24 | 2.53 | 2.30 | 1.77 | 1.63 | 8.97 | 1.64 |
| Hydrocarbon | | | | | | | |
| Alkane | | | | | | | |
| C4 - C12 | 3.66 | 5.48 | 6.95 | 31.54 | 5.98 | 6.12 | 7.60 |
| C13-C18 | 7.93 | 5.36 | 14.13 | 2.24 | 4.63 | 7.59 | 6.54 |
| Alkene | | | | | | | |
| C4 - C12 | 4.39 | 20.11 | 16.01 | 25.35 | 14.06 | 15.85 | 21.39 |
| C13-C18 | 25.18 | 22.86 | 27.68 | 9.22 | 32.77 | 18.96 | 20.84 |
| Alkyne | - | - | - | - | - | - | 2.01 |
| Others | 0.56 | 6.55 | 0.58 | 6.36 | - | 2.48 | - |

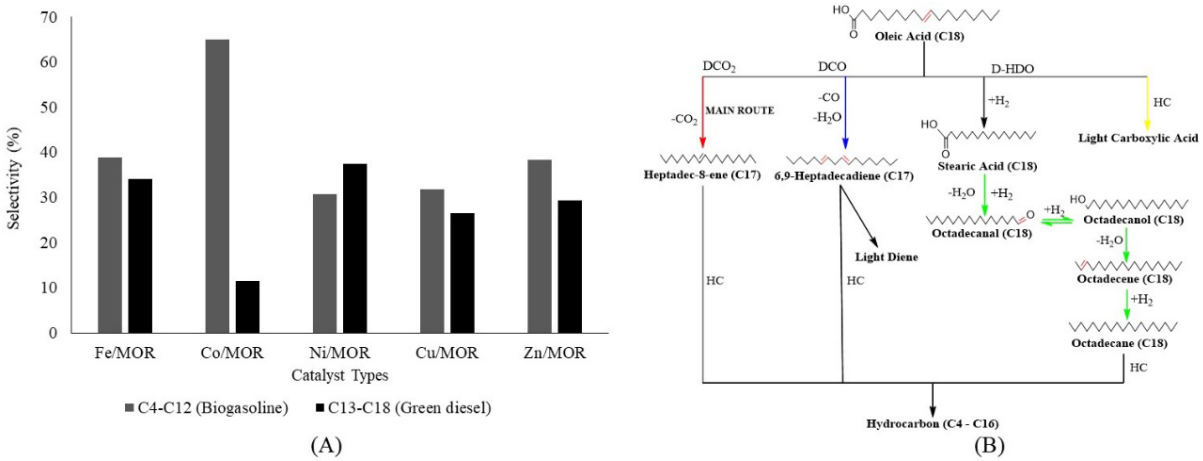


FIGURE 5. A) Selectivity of bio gasoline (C4-C12) and green diesel (C13-C18) fraction, B) Proposed schematic of oleic acid hydrodeoxygenation reaction

an HC reaction that reduces the selectivity of green diesel (Shim et al. 2015). The order of the selectivity of the catalyst in the production of biogasoline is as follows Co/MOR > Fe/MOR =Zn/MOR > Ni/MOR = Cu/MOR. This trend follows the Sabatier principle, which says that in one period, the elements in the middle have the optimum ability to interact with the reactants, not too strong or too weak. So that the reaction activity also becomes the most optimum as well.

The Lewis acid sites are derived from the nature of the metals, while the Bronsted acid sites depend on the number of OH groups or the Si/Al ratio on the mordenite surface (Arun, Sharma & Dalai 2015). The high Si/Al ratio decreases the acid concentration and the Bronsted/Lewis (B/L) proportion, resulting in a lower concentration of Brønsted acid sites. As a consequence, HC reactions tend to be minimized. In contrast, the green diesel selectivity is increased. The high Brønsted acid site increases the HC reaction in long-chain hydrocarbons (>C11). Therefore, a low Si/Al ratio catalyst produces more light hydrocarbons with fewer carbon atoms (Feng et al. 2019).

The following is the order of catalysts from the highest Si/Al ratio to the lowest Co/MOR>Ni/MOR>Cu/MOR>Fe/MOR. Co/MOR catalyst has the highest Si/Al ratio that causes low concentrations of Bronsted acid sites but high selectivity of C4-C6 as a cracking product (Tamiyakul et al. 2015). Therefore, the Co/MOR catalyst has a suitable acidity to activate the reactants due to its high selectivity of C4-C12.

## CONCLUSION

This paper reports the research results of the catalytic properties of TMs/MOR (with TMs = Fe, Co, Ni, Cu, and Zn). Although the highest conversion of oleic acid from the Co/MOR catalyzed reaction is 98.82%, Co/MOR is unsuitable as a catalyst for the oleic acid conversion into green diesel. Ni/MOR also shows the best selectivity for C13-C18 than others, while Co/MOR is suitable for C4-C12 (biogasoline). The high activity and green diesel selectivity of the Ni/MOR catalyst are due to the excellent interaction between Ni metal and mordenite, which activates the reactants to produce the desired product. Meanwhile, the direct reaction of HDO-HC and $DCO_2$ that dominates the HDO reaction is possible due to the high acidity of the catalyst. Our research shows that transition metal catalytic properties follow the Sabatier principle, which states that the element in the middle has the best ability to interact with the reactants, resulting in the best reaction activity.

## ACKNOWLEDGMENTS

We gratefully acknowledge the financial support of a project funded by Sebelas Maret University through a Fundamental Grant 2021-2022 (No. 316/UN27/HK/2022) and Ministry of Education, Culture, Research and Technology through a Regular Fundamental Grant 2024 (1076.1/UN27.22/PT.01.03/2024).

## REFERENCES

Ajeeb, W., Gomes, D.M., Neto, R.C. & Baptista, P. 2025. Life cycle analysis of hydrotreated vegetable oils production based on green hydrogen and used cooking oils. *Fuel* 390: 134749. https://doi.org/10.1016/J.FUEL.2025.134749

Aliana-Nasharuddin, N., Asikin-Mijan, N., Abdulkareem-Alsultan, G., Saiman, M.I., Alharthi, F.A. Alghamdi, A.A. & Taufiq-Yap, Y.H. 2019. Production of green diesel from catalytic deoxygenation of chicken fat oil over a series binary metal oxide-supported MWCNTs. *RSC Advances* 10(2): 626-642. https://doi.org/10.1039/c9ra08409f

Arun, N., Sharma, R.V. & Dalai, A.K. 2015. Green diesel synthesis by hydrodeoxygenation of bio-based feedstocks: Strategies for catalyst design and development. *Renewable and Sustainable Energy Reviews* 48: 240-255. https://doi.org/10.1016/j.rser.2015.03.074

Arun, N., Nanda, S., Hu, Y. & Dalai, A.K. 2021. Hydrodeoxygenation of oleic acid using γ-$Al_2O_3$ supported transition metallic catalyst systems: Insight into the development of novel FeCu/γ-$Al_2O_3$ catalyst. *Molecular Catalysis* 523: 111526. https://doi.org/10.1016/j.mcat.2021.111526

Asikin-Mijan, N., Juan, J.C., Taufiq-Yap, Y.H., Ong, H.C., Lin, Y.C., AbdulKareem-Alsultan, G. & Lee, H.V. 2023. Towards sustainable green diesel fuel production: Advancements and opportunities in acid-base catalyzed $H_2$-free deoxygenation process. *Catalysis Communications* 182: 106741. https://doi.org/10.1016/j.catcom.2023.106741

Ayodele, O.B. 2017. Influence of oxalate ligand functionalization on Co/ZSM-5 activity in Fischer Tropsch synthesis and hydrodeoxygenation of oleic acid into hydrocarbon fuels. *Scientific Reports* 7(1): 10008. https://doi.org/10.1038/s41598-017-09706-z

Bardestani, R., Patience, G.S. & Kaliaguine, S. 2019. Experimental methods in chemical engineering: Specific surface area and pore size distribution measurements—BET, BJH, and DFT. *The Canadian Journal of Chemical Engineering* 97(11): 2781-2791. https://doi.org/10.1002/cjce.23632

Carli, M.F., Susanto, B.H. & Habibie, T.K. 2018. Sythesis of bioavture through hydrodeoxygenation and catalytic cracking from oleic acid using NiMo/zeolit catalyst. *E3S Web of Conferences* 67: 02023. https://doi.org/10.1051/e3sconf/20186702023

Chen, L., Janssens, T.V.W., Skoglundh, M. & Grönbeck, H. 2019. Interpretation of $NH_3$-TPD profiles from Cu-CHA using first-principles calculations. *Topics in Catalysis* 62(1-4): 93-99. https://doi.org/10.1007/s11244-018-1095-y

Choo, M.Y., Oi, L.E., Ling, T.C., Ng, E.P., Lin, Y.C., Centi, G. & Juan, J.C. 2020. Deoxygenation of triolein to green diesel in the $H_2$-free condition: Effect of transition metal oxide supported on zeolite Y. *Journal of Analytical and Applied Pyrolysis* 147: 104797. https://doi.org/10.1016/j.jaap.2020.104797

Crawford, J.M., Zaccarine, S.F., Kovach, N.C., Smoljan, C.S., Lucero, J., Trewyn, B.G., Pylypenko, S. & Carreon, M.A. 2020. Decarboxylation of stearic acid over Ni/MOR catalysts. *Journal of Chemical Technology & Biotechnology* 95(1): 102-110. https://doi.org/10.1002/jctb.6211

de Oliveira Camargo, M., Willimann Pimenta, J.L.C., de Oliveira Camargo, M. & Arroyo, P.A. 2020. Green diesel production by solvent-free deoxygenation of oleic acid over nickel phosphide bifunctional catalysts: Effect of the support. *Fuel* 281: 118719. https://doi.org/10.1016/j.fuel.2020.118719

Douvartzides, S.L., Charisiou, N.D., Papageridis, K.N. & Goula, M.A. 2019. Green diesel: Biomass feedstocks, production technologies, catalytic research, fuel properties and performance in compression ıgnition ınternal combustion engines. *Energies* 12(5): 809. https://doi.org/10.3390/en12050809

Feng, F., Wang, L., Zhang, X. & Wang, Q. 2019. Selective hydroconversion of oleic acid into aviation-fuel-range alkanes over ultrathin Ni/ZSM-5 nanosheets. *Industrial and Engineering Chemistry Research* 58(14): 5432-5444. https://doi.org/10.1021/acs.iecr.9b00103

Hafriz, R.S.R.M., Nor Shafizah, I., Salmiaton, A., Arifin, N.A., Yunus, R., Taufiq Yap, Y.H. & Abd Halim, S. 2020. Comparative study of transition metal-doped calcined Malaysian dolomite catalysts for WCO deoxygenation reaction. *Arabian Journal of Chemistry* 13(11): 8146-8159. https://doi.org/10.1016/j.arabjc.2020.09.046

Haryani, N., Harahap, H., Taslim & Irvan. 2020. Biogasoline production via catalytic cracking process using zeolite and zeolite catalyst modified with metals: A review. *IOP Conference Series: Materials Science and Engineering* 801: 012051. https://doi.org/10.1088/1757-899X/801/1/012051

Hongloi, N., Prapainainar, P. & Prapainainar, C. 2022. Review of green diesel production from fatty acid deoxygenation over Ni-based catalysts. *Molecular Catalysis* 523: 111696. https://doi.org/10.1016/J.MCAT.2021.111696

Hongloi, N., Prapainainar, P., Seubsai, A., Sudsakorn, K. & Prapainainar, C. 2019. Nickel catalyst with different supports for green diesel production. *Energy* 182: 306-320. https://doi.org/10.1016/j.energy.2019.06.020

I. Istadi, Rahma Amalia, Teguh Riyanto, Didi D. Anggoro, Bunjerd Jongsomjit & Ari Bawono Putranto. 2022. Acids treatment for ımproving catalytic properties and activity of the spent RFCC catalyst for cracking of palm oil to kerosene-diesel fraction fuels. *Molecular Catalysis* 527: 112420. https://doi.org/10.1016/J.MCAT.2022.112420

Janampelli, S. & Darbha, S. 2019. Highly efficient Pt-MoOx/ZrO2 catalyst for green diesel production. *Catalysis Communications* 125: 70-76. https://doi.org/10.1016/j.catcom.2019.03.027

Jeon, K.W., Na, H.S., Lee, Y.L., Ahn, S.Y., Kim, K.J., Shim, J.O., Jang, W.J., Jeong, D.W., Nah, I.W. & Roh, H.S. 2019a. Catalytic deoxygenation of oleic acid over a Ni-$CeZrO_2$ catalyst. *Fuel* 258: 116179. https://doi.org/10.1016/j.fuel.2019.116179

Jeon, K-W., Shim, J-O., Jang, W-J., Lee, D.W., Na, H-S., Kim, H-M., Lee, Y-L., Yoo, S-Y., Roh, H-S., Jeon, B-H., Bae, J.W. & Ko, C.H. 2019b. Effect of calcination temperature on the association between free NiO species and catalytic activity of Ni–$Ce_{0.6}Zr_{0.4}O_2$ deoxygenation catalysts for biodiesel production. *Renewable Energy* 131: 144-151. https://doi.org/10.1016/j.renene.2018.07.042

Jing, Z-Y., Zhang, T-Q., Shang, J-W., Zhai, M-L., Yang, H., Qiao, C-Z. & Ma, X-Q. 2018. Influence of Cu and Mo components of γ-$Al_2O_3$ supported nickel catalysts on hydrodeoxygenation of fatty acid methyl esters to fuel-like hydrocarbons. *Journal of Fuel Chemistry and Technology* 46(4): 427-440. https://doi.org/10.1016/S1872-5813(18)30018-5

Kamaruzaman, M.F., Taufiq-Yap, Y.H. & Derawi, D. 2020. Green diesel production from palm fatty acid distillate over SBA-15-supported nickel, cobalt, and nickel/cobalt catalysts. *Biomass and Bioenergy* 134: 105476. https://doi.org/10.1016/j.biombioe.2020.105476

Kochaputi, N., Kongmark, C., Khemthong, P., Butburee, T., Kuboon, S., Worayingyong, A. & Faungnawakij, K. 2019. Catalytic behaviors of supported Cu, Ni, and Co phosphide catalysts for deoxygenation of oleic acid. *Catalysts* 9(9): 715. https://doi.org/10.3390/catal9090715

Kordulis, C., Bourikas, K., Gousi, M., Kordouli, E. & Lycourghiotis, A. 2016. Development of nickel based catalysts for the transformation of natural triglycerides and related compounds into green diesel: A critical review. *Applied Catalysis B: Environmental* 181: 156-196. https://doi.org/10.1016/j.apcatb.2015.07.042

Li, W., Li, F., Wang, H., Liao, M., Li, P., Zheng, J., Tu, C. & Li, R. 2020. Hierarchical mesoporous ZSM-5 supported nickel catalyst for the catalytic hydrodeoxygenation of anisole to cyclohexane. *Molecular Catalysis* 480: 110642. https://doi.org/10.1016/j.mcat.2019.110642

Luciano, V.A., de Paula, F.G., Pinto, P.S., Prates, C.D., Pereira, R.C.G., Ardisson, J.D., Rosmaninho, M.G. & Teixeira, A.P.C. 2022. Thermal cracking of oleic acid promoted by ıron species from ıron ore tailings for the production of ketones and fuels. *Fuel* 310(Part A): 122290. https://doi.org/10.1016/j.fuel.2021.122290

Mazlan, Nugrahaningtyas, K.D. & Rahmawati, F. 2022. Effect of Fe metal loading on the character of HZSM-5. *AIP Conference Proceedings* 2391: 050011. https://doi.org/10.1063/5.0072981

Miao, C., Zhou, G., Chen, S., Xie, H. & Zhang, X. 2020. Synergistic effects between Cu and Ni species in NiCu/γ-$Al_2O_3$ catalysts for hydrodeoxygenation of methyl laurate. *Renewable Energy* 153: 1439-1454. https://doi.org/10.1016/j.renene.2020.02.099

Mirzayanti, Y.W., Kurniawansyah, F., Prajitno, D.H. & Roesyadi, A. 2018. Zn-Mo/HZSM-5 catalyst for gasoil range hydrocarbon production by catalytic hydrocracking of *Ceiba pentandra* oil. *Bulletin of Chemical Reaction Engineering & Catalysis* 13(1): 136-143. https://doi.org/10.9767/bcrec.13.1.1508.136-143

Morgan, A.S., Hossain, M.Z., Chowdhury, M.B.I. & Charpentier, P. 2024. $ScCO_2$ decarboxylation of oleic acid to green diesel. *The Journal of Supercritical Fluids* 205: 106120. https://doi.org/10.1016/J.SUPFLU.2023.106120

Na, J.G., Yi, B.E., Kim, J.N., Yi, K.B., Park, S.Y., Park, J.H., Kim, J.N. & Ko, C.H. 2010. Hydrocarbon production from decarboxylation of fatty acid without hydrogen. *Catalysis Today* 156(1-2): 44-48. https://doi.org/10.1016/j.cattod.2009.11.008

Neonufa, G.F., Soerawidjaja, T.H., Indarto, A. & Prakoso, T. 2019. An ınnovative technique to suppress alkene-bond in green diesel by Mg–Fe basic soap thermal decarboxylation. *International Journal of Ambient Energy* 40(4): 374-380. https://doi.org/10.1080/01430750.2017.1399451

Nugraha, R.E., Purnomo, H., Aziz, A., Holilah, H., Bahruji, H., Asikin-Mijan, N., Suprapto, S., Taufiq-Yap, Y.H., Abdul Jalil, A., Hartati, H. & Prasetyoko, D. 2024. The mechanism of oleic acid deoxygenation to green diesel hydrocarbon using porous aluminosilicate catalysts. *South African Journal of Chemical Engineering* 49: 122-135. https://doi.org/10.1016/J.SAJCE.2024.04.009

Nugrahaningtyas, K.D., Putri, M.M. & Saraswati, T.E. 2020. Metal phase and electron density of transition Metal/HZSM-5. *AIP Conference Proceedings* 2237: 020003. https://doi.org/10.1063/5.0005561

Nugrahaningtyas, K.D., Hidayat, Y., Lukitawati, R., Mukhsin, S.A. & Sabiilagusti, A.I. 2022a. The effect of hydrogen flow rate and temperature on hydrodeoxygenation of oleic acid over Ni/MOR catalysts. *AIP Conference Proceedings* 2022: 020041. https://doi.org/10.1063/5.0111684

Nugrahaningtyas, K.D., Kurniawati, M.F., Masykur, A. & 'Abidah Quratul'aini. N. 2022b. Periodic trends in the character of first-row transition metals-based catalysts embedded on mordenite. *Moroccan Journal of Chemistry* 10(3): 375-386. https://doi.org/10.48317/IMIST.PRSM/morjchem-v10i3.30900

Nugrahaningtyas, K.D., Suharbiansah, R.S.R., Lestari, W.W. & Rahmawati, F. 2022c. Metal phase, electron density, textural properties, and catalytic activity of CoMo based catalyst applied in hydrodeoxygenation of oleic acid. *Evergreen* 9(2): 283-291. https://doi.org/10.5109/4793665

Nugrahaningtyas, K.D., Heraldy, E., Rachmadani, Hidayat, Y. & Kartini, I. 2021. Effect of synthesis and activation methods on the character of CoMo/ ultrastable Y-Zeolite catalysts. *Open Chemistry* 19(1): 745-754. https://doi.org/10.1515/chem-2021-0064

Nugrahaningtyas, K.D., Putri, I.F., Heraldy, E. & Hidayat, Y. 2018. The catalytic activity of CoMo/ USY on deoxygenation reaction of anisole in a batch reactor. *IOP Conference Series: Materials Science and Engineering* 349: 012030. https://doi.org/10.1088/1757-899X/349/1/012030

Nur Azreena, I., Asikin-Mijan, N., Lau, H.L.N., Hassan, M.A., Mohd Izham, S., Kennedy, E., Stockenhuber, M., Yan, P. & Taufiq-Yap, Y.H. 2024. Hydro-processing of palm fatty acid distillate for diesel-like hydrocarbon fuel production using La-zeolite beta catalyst. *Industrial Crops and Products* 218: 118907. https://doi.org/10.1016/j.indcrop.2024.118907

Nur Azreena, I., Lau, H.L.N., Asikin-Mijan, N., Hassan, M.A., Mohd Izham, S., Kennedy, E., Stockenhuber, M., Mastuli, M.S., Alharthi, F.A., Alghamdi, A.A. & Taufiq-Yap, Y.H. 2021. A promoter effect on hydrodeoxygenation reactions of oleic acid by zeolite beta catalysts. *Journal of Analytical and Applied Pyrolysis* 155: 105044. https://doi.org/10.1016/j.jaap.2021.105044

Orozco, L.M., Echeverri, D.A., Sánchez, L. & Rios, L.A. 2017. Second-generation green diesel from castor oil: Development of a new and efficient continuous-production process. *Chemical Engineering Journal* 322: 149-156. https://doi.org/10.1016/j.cej.2017.04.027

Oyedotun, T.D.T. 2018. X-ray fluorescence (XRF) in the ınvestigation of the composition of earth materials: A review and an overview. *Geology, Ecology, and Landscapes* 2(2): 148-154. https://doi.org/10.1080/24749508.2018.1452459

Panchuk, V., Yaroshenko, I., Legin, A., Semenov, V. & Kirsanov, D. 2018. Application of chemometric methods to XRF-data - A tutorial review. *Analytica Chimica Acta* 1040: 19-32. https://doi.org/10.1016/j.aca.2018.05.023

Pazmiño-Viteri, K., Cabezas-Terán, K., Echeverría, D., Cabrera, M. & Taco-Vásquez, S. 2024. Average carbon number analysis and relationship with octane number and PIONA analysis of premium and regular gasoline expended in Ecuador. *Processes* 12(8): 1706. https://doi.org/10.3390/pr12081706

Pourzolfaghar, H., Abnisa, F., Wan Daud, W.M.A. & Aroua, M.K. 2020. Gas-phase hydrodeoxygenation of phenol over Zn/$SiO_2$ catalysts: Effects of zinc load, temperature, weight hourly space velocity, and $H_2$ volumetric flow rate. *Biomass and Bioenergy* 138: 105556. https://doi.org/10.1016/J.BIOMBIOE.2020.105556

Prakhar, A., Ojagh, H., Woo, J., Grennfelt, E.L., Olsson, L. & Creaser, D. 2018. Investigating the effect of Fe as a poison for catalytic HDO over sulfided NiMo alumina catalysts. *Applied Catalysis B: Environmental* 227: 240-251. https://doi.org/10.1016/j.apcatb.2018.01.027

Puspawiningtiyas, E., Prakoso, T., Pratiwi, M., Subagjo, S. & Soerawidjaja, T.H. 2022. Production of biogasoline via pyrolysis of oleic acid basic soaps. *Journal of Engineering and Technological Sciences* 54(3): 220311. https://doi.org/10.5614/J.ENG.TECHNOL.SCI.2022.54.3.11

Rogers, K.A. & Zheng, Y. 2016. Selective deoxygenation of biomass-derived bio-oils within hydrogen-modest environments: A review and new ınsights. *ChemSusChem* 9(14): 1750-1772. https://doi.org/10.1002/cssc.201600144

Safa Gamal, M., Asikin-Mijan, N., Wan Khalit, W.N.A., Arumugam, M., Mohd Izham, S. & Taufiq-Yap, Y.H. 2020. Effective catalytic deoxygenation of palm fatty acid distillate for green diesel production under hydrogen-free atmosphere over bimetallic catalyst CoMo supported on activated carbon. *Fuel Processing Technology* 208: 106519. https://doi.org/10.1016/j.fuproc.2020.106519

Sakizci, M. & Kılınç, L.Ö. 2015. Influence of acid and heavy metal cation exchange treatments on methane adsorption properties of mordenite. *Turkish Journal of Chemistry* 39(5): 970-983. https://doi.org/10.3906/kim-1501-71

Shim, J-O., Jeong, D-W., Jang, W-J., Jeon, K-W., Kim, S-H., Jeon, B-H., Roh, H-S., Na, J-G., Oh, Y-K., Han, S.S. & Ko, C.H. 2015. Optimization of unsupported CoMo catalysts for decarboxylation of oleic acid. *Catalysis Communications* 67: 16-20. https://doi.org/10.1016/j.catcom.2015.03.034

Siraj, M. & Ceylan, S. 2025. Investigation of the effect of catalyst support on oleic acid catalytic deoxygenation for green diesel production. *Journal of Porous Materials* 32: 941-952. https://doi.org/10.1007/S10934-024-01725-2

Tamiyakul, S., Ubolcharoen, W., Tungasmita, D.N. & Jongpatiwut, S. 2015. Conversion of glycerol to aromatic hydrocarbons over Zn-promoted HZSM-5 catalysts. *Catalysis Today* 256(P2): 325-335. https://doi.org/10.1016/j.cattod.2014.12.030

Taromi, A.A. & Kaliaguine, S. 2018. Green diesel production via continuous hydrotreatment of triglycerides over mesostructured γ-alumina supported NiMo/CoMo catalysts. *Fuel Processing Technology* 171: 20-30. https://doi.org/10.1016/j.fuproc.2017.10.024

Wang, F., Xu, J., Jiang, J., Liu, P., Li, F., Ye, J. & Zhou, M. 2018. Hydrotreatment of vegetable oil for green diesel over activated carbon supported molybdenum carbide catalyst. *Fuel* 216: 738-746. https://doi.org/10.1016/j.fuel.2017.12.059

Zdainal Abidin, S.N., Lee, H.V., Asikin-Mijan, N., Juan, J.C., Abd Rahman, N., Mastuli, M.S., Taufiq-Yap, Y.H. & Kong, P.S. 2019. Ni, Zn and Fe hydrotalcite-like catalysts for catalytic biomass compound into green biofuel. *Pure and Applied Chemistry* 92(4): 587-600. https://doi.org/10.1515/pac-2019-0820

Zhang, Z., Bi, G., Zhang, H., Zhang, A., Li, X. & Xie, J. 2019. Highly active and selective hydrodeoxygenation of oleic acid to second generation bio-diesel over $SiO_2$-supported CoxNi1−xP catalysts. *Fuel* 247: 26-35. https://doi.org/10.1016/j.fuel.2019.03.021

Zhao, X., Wei, L., Cheng, S., Cao, Y., Julson, J. & Gu, Z. 2015. Catalytic cracking of carinata oil for hydrocarbon biofuel over fresh and regenerated Zn/Na-ZSM-5. *Applied Catalysis A: General* 507: 44-55. https://doi.org/10.1016/J.APCATA.2015.09.031

Zheng, Y., Wang, J., Liu, C., Lu, Y., Lin, X., Li, W. & Zheng, Z. 2020. Efficient and stable Ni-Cu catalysts for *ex situ* catalytic pyrolysis vapor upgrading of oleic acid into hydrocarbon: Effect of catalyst support, process parameters and Ni-to-Cu mixed ratio. *Renewable Energy* 154: 797-812. https://doi.org/10.1016/j.renene.2020.03.058

*Corresponding author; email: khoirinadwi@staff.uns.ac.id

SUPPLEMENTARY 1. The XRD diffraction pattern using the Le Bail method with RIETICA software

(1) Mordenite #4393

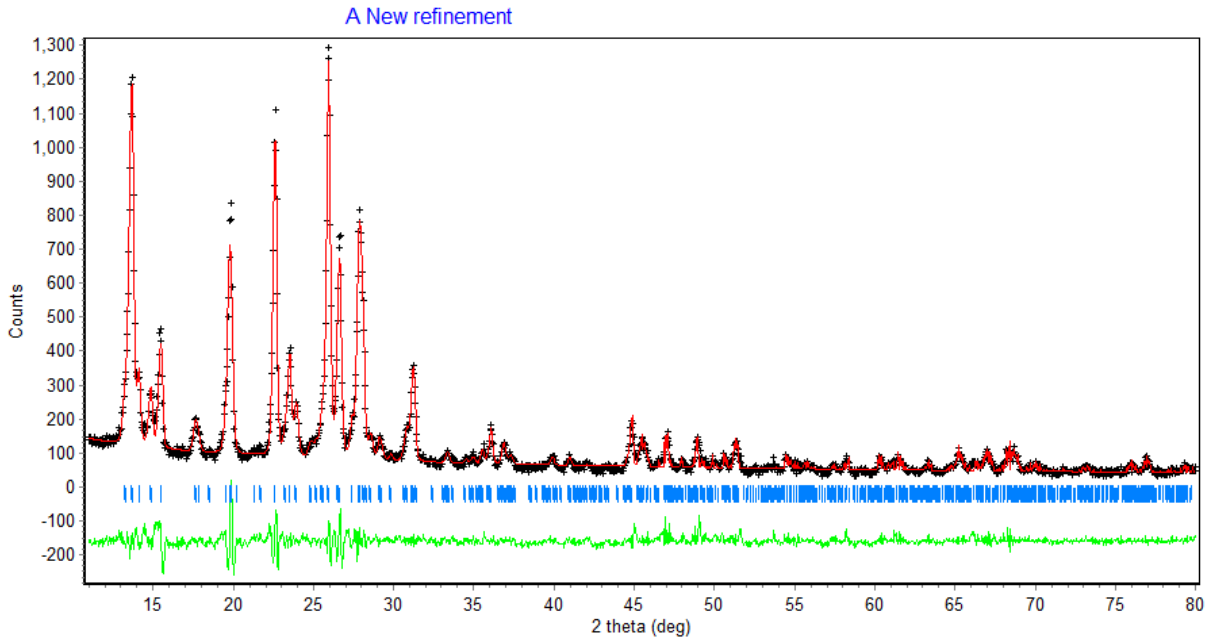


Le Bail plot of X-ray diffraction data of mordenite with mordenite standard. Experimental data (+); calculated result(---); difference between experimental data and calculated result (---). Rp and Rwp values are 8.11 and 8.18%, respectively.

(2) Mordenite #4393 #4394

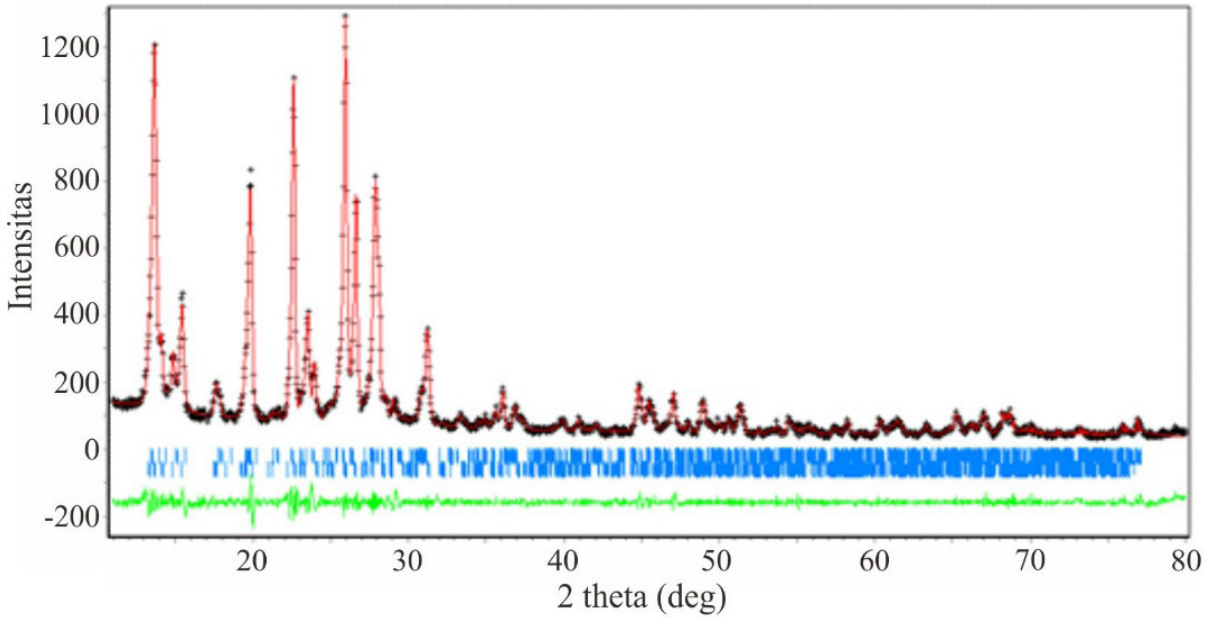


Le Bail plot of X-ray diffraction data of mordenite with mordenite standard. Experimental data (+); calculated result(---); difference between experimental data and calculated result (---). Rp and Rwp values are 5.89 and 5.13%, respectively.

SUPPLEMENTARY 2. The XRD diffraction pattern using the Le Bail method with RIETICA software

a. Fe/MOR catalyst plotted against the ICSD standard with numbers #4393 #4394 #41506 #20596 #24695

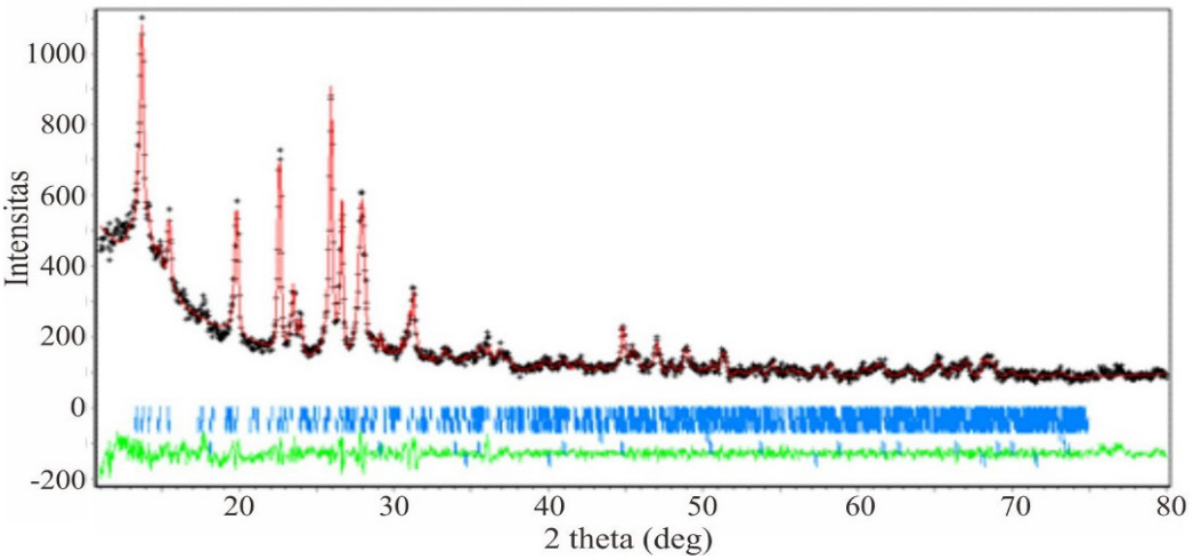


Le Bail plot of X-ray diffraction data of mordenite with mordenite standard. Experimental data (+); calculated result(---); difference between experimental data and calculated result (---). Rp and Rwp values are 5.69 and 5.64 %, respectively.

b. Co/MOR catalyst plotted against the ICSD standard with numbers #4393 #4394 #41507 #43458 #24210 #87942 #93858

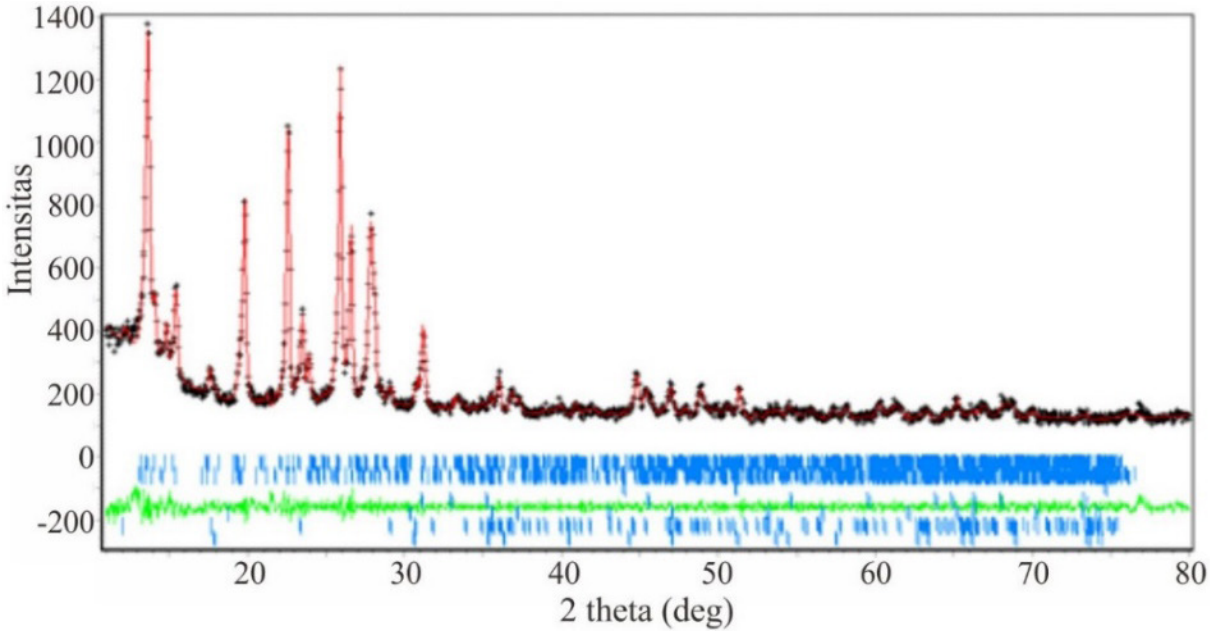


Le Bail plot of X-ray diffraction data of mordenite with mordenite standard. Experimental data (+); calculated result(---); difference between experimental data and calculated result (---). Rp and Rwp values are 4.60 and 5.05%, respectively.

c. Ni/MOR catalyst plotted against the ICSD standard with numbers #4393; #4394, #41508; #92127, and #78698

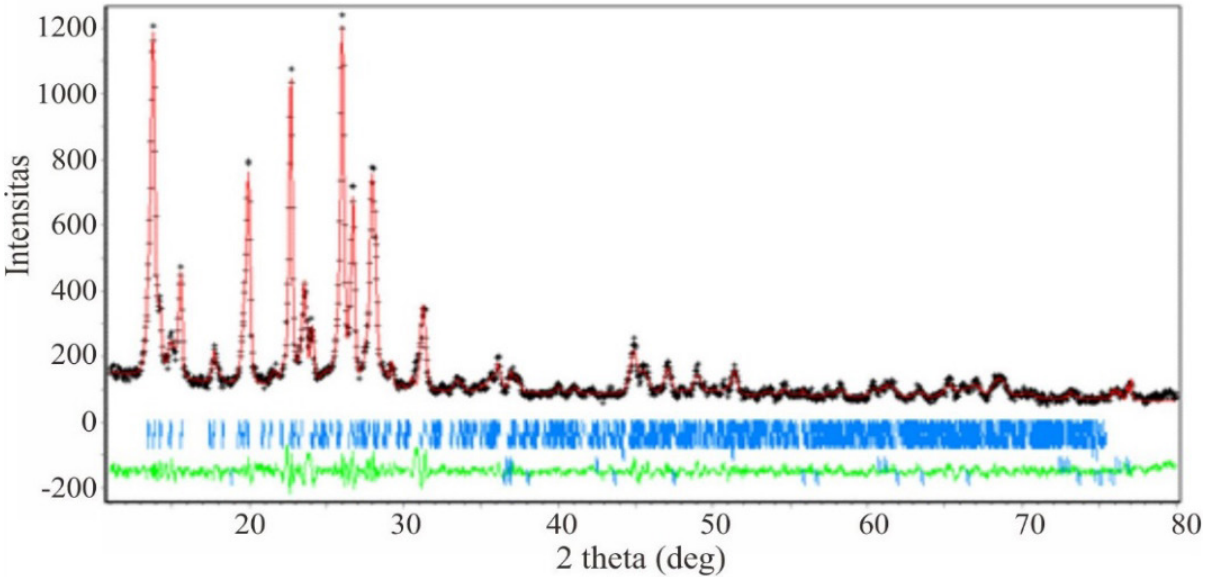


Le Bail plot of X-ray diffraction data of mordenite with mordenite standard. Experimental data (+); calculated result(---); difference between experimental data and calculated result (---). Rp and Rwp values are 6.94 and 5.59%, respectively.

d. Cu/MOR catalyst plotted against the ICSD standard with numbers #4393; #4394; #; #61323; #26963; and #54126

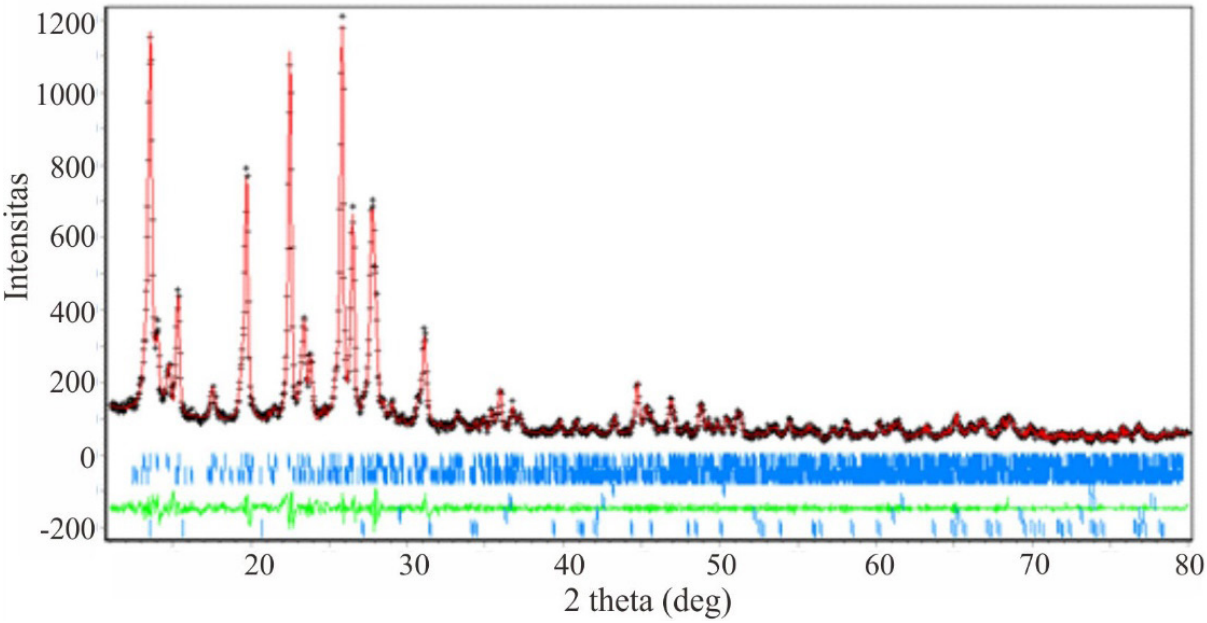


Le Bail plot of X-ray diffraction data of mordenite with mordenite standard. Experimental data (+); calculated result(---); difference between experimental data and calculated result (---). Rp and Rwp values are 4.98 and 4.99%, respectively.

e. Zn/MOR catalyst plotted against the ICSD standard with numbers #4393; #4394; and #57156

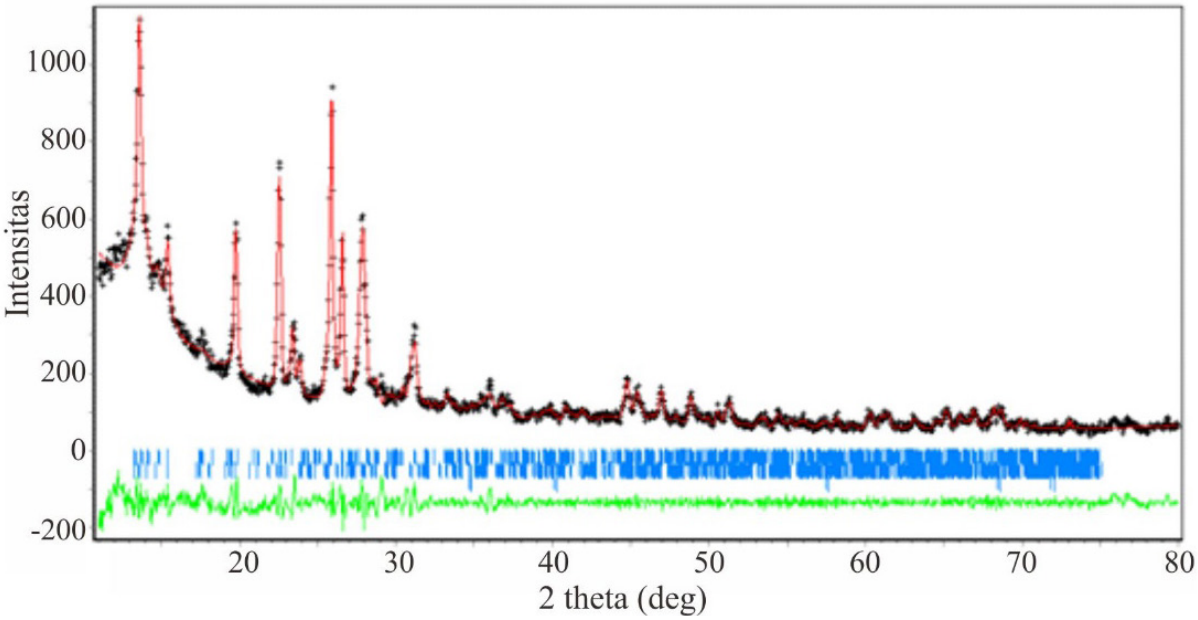


Le Bail plot of X-ray diffraction data of mordenite with mordenite standard. Experimental data (+); calculated result(---); difference between experimental data and calculated result (---). Rp and Rwp values are 6.48 and 6.10 %, respectively.